Appl. Phys. B 82, 19–24 (2006)
DOI: 10.1007/s00340-005-1994-z

Applied Physics B
Lasers and Optics

A.I. MAGUNOV[1]
D. BATANI[3,✉]
A.Y. FAENOV[2]
G. LUCCHINI[3]
T. DESAI[3]
F. PADOAN[3]
T.A. PIKUZ[2]
I.Y. SKOBELEV[2]
F. CANOVA[3]
N. CHIODINI[4]

Characterization of compact bright soft X-ray source based on picosecond laser plasma

[1] A.M. Prokhorov General Physics Institute, Russian Academy of Sciences, 119991 Moscow, Russia
[2] Multicharged Ions Spectra Data Center of VNIIFTRI, Mendeleevo, 141570 Moscow region, Russia
[3] Dipartimento di Fisica "G. Occhialini", Università degli Studi di Milano-Bicocca, 20126 Milano, Italy
[4] Dipartimento di Scienza dei Materiali, Università degli Studi di Milano-Bicocca, 20126 Milano, Italy

Received: 20 April 2005/Revised version: 16 August 2005
Published online: 23 November 2005 •

ABSTRACT Radiation emission of silicon and aluminum plasmas produced by 40-ps laser pulses with peak intensity above 10^{14} W/cm^2 was studied. High-resolution soft X-ray spectra of H-like and He-like ions were analyzed to determine plasma parameters. We compared the line shape of resonance transitions and their intensity ratios to corresponding dielectronic satellites and the intensities of the intercombination lines of He-like ions with the results of model calculations. Such comparisons gave average values of the electron number density $N_e = (1-1.9) \times 10^{21}$ cm^{-3} and the electron temperature $T_e = 460$–560 eV for Si plasmas and about 560 eV for Al plasmas produced by the first and the second laser harmonics. The plasma size is about 100 μm. According to our estimations, more than 10^{12} photons were produced within the resonance line spectral width and in the solid angle 2π during the total decay period.

PACS 41.50.+h; 52.25.Os; 52.50.Jm

1 Introduction

Hot and dense laser-produced plasmas are objects worth investigating for several reasons. They are powerful sources of short wavelength radiation and fast charged particles. Furthermore, they play a key role in the context of inertial confinement fusion. They also are unique tools to study fundamental properties of matter subject to high-energy concentration (high- energy density matter).

From the point of view of applications, laboratory laser–plasma X-ray sources have already been applied in radiobiology [1–4], X-ray microscopy [5–8], and microlithography [9, 10]. The knowledge of X-spectra formation is very important for all these applications. For instance in micro-lithography, X-ray photons of about 1-keV energy are required to achieve efficient radiation transfer through the X-ray mask membrane and sufficient energy deposition onto the resist-coated Si wafer. In radiobiology, laser–plasma X-ray sources were used to irradiate biological specimens: V-79 Chinese hamster cells [1] for studying DNA damage, DNA repair, and repair inhibition, or Saccharomices Cerevisiae yeast cells [2, 3] for studying metabolic damages. In the first case, X-rays at $h\nu \approx 1.2$ keV were produced using L-shell emission from Cu targets. These could penetrate to the cell nucleus so that the absorbed dose was really related to DNA damage. In the second case, low-energy X-ray photons were needed to deposit the dose at the cell wall so that damages at the metabolic level without touching the cell nucleus could be produced. Finally in X-ray microscopy, only X-rays in the "water window" (between 22 and 44 Å) will contribute to the formation of a clean image, being absorbed by the biological material but not by water. The presence of other X-ray lines will blur the image contrast dramatically.

Besides all this, the study of X-ray spectra from plasmas is a subject rewarding by itself and hence a well developed field in physics. Indeed on the one side, X-ray spectra are very important for atomic physics because by recording X-ray emission lines, one can access the energy levels in atoms and multi-charged ions [26–28]. On the other hand, X-ray spectroscopy is a key technique in plasma diagnostics [30–32] since from measurements of X-ray spectra plasma parameters like electron density, electron temperature, and ion charges can be obtained. Even information on plasma opacities and the exact shape of the electron distribution function (including the presence of fast electrons) can be deduced. In particular, high-precision X-ray radiation spectroscopy is a very sensitive tool for the diagnostics of hot and dense plasmas, when line shapes and relative intensities of the resonance transitions and their dielectronic satellites from multicharged ions are used.

Many recent laser–plasma investigations have focused on ultra-short processes with femtosecond laser pulses. However, as the plasma decay period is much longer than the laser pulse duration, the X-ray emission yield in time-integrated emission spectra is dominated by the plasma expansion period. In this case, the problem is how to extract the information about the short laser–plasma interaction from the resulting spectrum, the available temporal resolution being limited usually to 0.5 ps. Measurements performed with picosecond laser pulses may hence be more convenient for spectroscopic investigations of laser–plasma processes.

The most intense soft X-ray emission from laser-produced plasmas is provided by the resonance transitions in the H-like and He-like ions and other many-electron ions with nearly closed electronic shells (Ne-like, Ni-like, etc.). At the same

✉ Fax: + 39 02 6448 2585; E-mail: batani@mib.infn.it

time, such transitions are very convenient for spectroscopic studies due to their relatively simple line structures, the availability of data on atomic structures and pertinent kinetic processes.

This paper presents the results obtained by analysing X-ray time-integrated spectra from Al and Si plasmas produced by 40-ps laser pulses. The experimentally observed line profiles of the resonance transitions in the H-like and He-like ions are compared with model calculations. The observations provide the relative intensities of dielectronic satellite lines, which are also used for the determination of the electron temperature by comparison with calculations. In this case, the plasma opacity effect has also been taken into account. The same spectral region was studied earlier with nanosecond plasmas in [11–15] and, more recently for Al, in the picosecond range [16].

2 Experimental setup and data processing

The experiments were performed at the University of Milano-Bicocca using a Nd:YAG laser system delivering 40-ps pulses with a typical energy of 40 mJ in the first and 20 mJ in the second harmonic. The first harmonic pulse actually contains a short train of "prepulses" with a typical 1 : 100 contrast to the main pulse, which are produced by leakage through the polarizer at each round-trip of the laser pulse in the cavity, before the main pulse is extracted by cavity dumping. When the second harmonic is used, such low-intensity prepulses are practically eliminated by non-linear frequency conversion.

The laser radiation was focused in a spot of 12 μm in diameter, thus the peak intensity in the pulse was about 5×10^{14} W cm^{-2} for the first harmonic and about 2.5×10^{14} W cm^{-2} for the second one. A more detailed description of the laser system can be found in [7]. The laser beam was focused with a lens on the target surface using incidence angles of 90° and 45°, which were changed by rotating the target. The simplified scheme of the experiment is shown in Fig. 1.

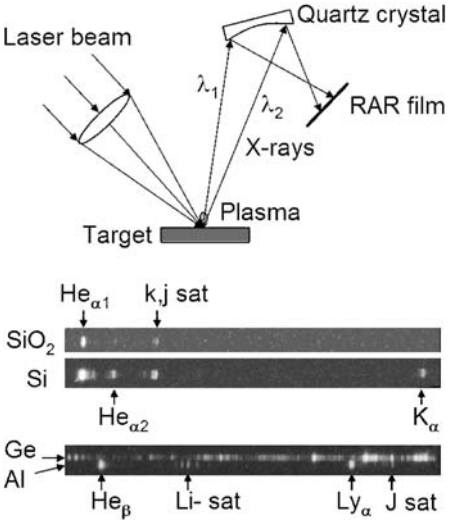

FIGURE 1 *Top*: Schematics of the experimental setup for laser-plasma X-ray spectroscopy measurements. *Bottom*: Several spectra images on the RAR film for different targets

The X-ray spectra were measured using focusing spherically bent quartz crystal spectrometers with a spatial resolution (FSSR) in the 2D-scheme [18]. The curvature radius of the crystal surface was 100 mm. Two spectrometers were aligned for different X-ray spectral regions at the observation angle of 70° to the target surface. The typical spectral resolution was $\lambda/\Delta\lambda_{\text{instr}} \approx 3000$ and the spatial resolution was about 15 μm. The X-ray spectra of the laser-produced plasmas were recorded in the first Bragg reflection order on RAR 2492 film. A PA filter (2-μm C_3H_6 film coated with 0.2-μm Al on both sides) was used to cut off the visible and VUV radiation. An additional Be-filter was used to attenuate the soft X-ray radiation in the region from 0.5 to 0.75 nm.

The spectra recorded on film, shown at the bottom of Fig. 1, were scanned and transformed into a optical density plot and finally to an intensity plot using the standard density and intensity calibration curves. These were corrected by taking into account the absorption of the filters and the reflection of the quartz crystal. The spectral dependence of the reflectivity of the spherically bent quartz crystal in the spectral region of the resonant He_α and characteristic K_α lines of silicon was taken from [19].

The spatial distribution of the X-ray radiation intensity on the films (the vertical direction in Fig. 1) corresponds to the average size of the plasma emission zone and is typically less than 200 μm.

3 Results and discussion

3.1 *Experimental data*

Different silicon materials were used as targets. Figure 2 shows a comparison of the first-harmonic-plasma spectra obtained from these targets with the spectrometers aligned in order to detect the spectral region between the He_α line of He-like silicon and the characteristic K_α line. The line labeling and spectroscopic constants of corresponding transitions are shown in Table 1. The results show a reduction of the total X-ray yield when the concentration of the silicon atoms in the targets (see curve 1, glass, and curve 4, SiO_2-aerogel)

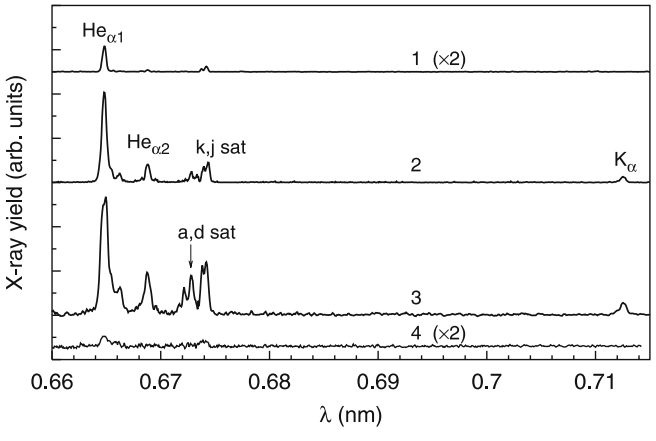

FIGURE 2 Experimentally observed X-ray spectra of Si ions in the glass plasma (*curve* 1), in the pure silicon plasma produced by the first laser harmonic (*curve* 2) and by the second harmonic (*curve* 3), and in the SiO_2-aerogel plasma (*curve* 4). The line notations are given in Table 1

Ion	Transition $i \rightarrow j$ (line key)	λ_{ij}	A_{ij}
Si^{+12}	$1s2p\,^1P_1 - 1s^2\,^1S_0$ ($He_{\alpha 1}$)	0.6648	3.76
	$1s2p\,^3P_1 - 1s^2\,^1S_0$ ($He_{\alpha 2}$)	0.6688	0.0157
Si^{+11}	$1s2p^2\,^2D_{5/2} - 1s^2 2p\,^2P_{3/2}$ (j)	0.6742	9.81[a]
	$1s2p^2\,^2D_{3/2} - 1s^2 2p\,^2P_{1/2}$ (k)	0.6738	6.61[a]
	$1s2p^2\,^2P_{3/2} - 1s^2 2p\,^2P_{3/2}$ (a)	0.6727	1.26[a]
	$1s2p^2\,^2P_{3/2} - 1s^2 2p\,^2P_{1/2}$ (d)	0.6727	0.045[a]
Al^{+12}	$2p\,^2P_{3/2} - 1s\,^2S_{1/2}$ ($Ly_{\alpha 1}$)	0.7171	1.787
	$2p\,^2P_{1/2} - 1s\,^2S_{1/2}$ ($Ly_{\alpha 2}$)	0.7176	1.792
Al^{+11}	$1s3p\,^1P_1 - 1s^2\,^1S_0$ ($He_{\beta 1}$)	0.6634	0.569
	$2p^2\,^1D_2 - 1s2p\,^1P_1$ (J)	0.7274	15.4[a]

[a] $q_{ij} = A_{ij}\Gamma_i/(\Sigma_k A_{ik} + \Gamma_i)$

TABLE 1 Spectroscopic constants for observed transitions in the Si and Al ions. λ_{ij} is the wavelength in nm, A_{ij} is the transition probability (in units 10^{13} s^{-1}), and Γ_i is the autoionization rate

is decreased. The SiO_2-aerogel is silica with a mass density of the order of 0.05 g/cm^3.

The characteristic K_α line was observed only with pure silicon targets (curves 2 and 3 in Fig. 2). Note, that K_α emission can be induced in the "cold" region of the target by inner-shell ionization of the Li-like and lower charged ions, either by hot electrons or by X-rays generated in the hot plasma corona. At the laser intensities used in our experiment, a maximum fast-electron energy of about 17 keV follows from the resonant absorption model. This is in fair agreement with measurements of the fast-electron temperature reported in literature at a laser wavelength of 1 μm and an intensity of 5×10^{14} W/cm^2. At the second harmonic, the fast-electron energy should be about 10 keV. Although the penetration of such electrons in Si is known, it is difficult to estimate the size of the K_α emitting region because the spectrometer gives the source size only in the transverse direction. As the measured K_α yield at the first and second laser harmonics are nearly equal, it seems more likely that K_α photons are produced by X-rays, rather than by fast electrons. The fact that K_α emission is observed only with pure Si targets is, probably, simply the result of the higher Si concentration in the target.

Curve 3 in Fig. 2 shows X-ray spectra from pure Si plasmas produced by the second harmonic pulse. The main difference from the spectrum at the first harmonic (curve 2) is the relative intensities of the $He_{\alpha 2}$ line and the *k* and *j* dielectronic satellites with respect to the $He_{\alpha 1}$ line. The peak intensity of the $He_{\alpha 1}$ line is nearly the same for the two laser frequencies. The laser intensity on the targets differs by a factor of 1.4 due to the difference in pulse energy and incidence angle. The intensities of the $He_{\alpha 2}$ and satellite lines is about three times larger for the second harmonic than for the first one.

We have also measured the emission from a SiO_2-aerogel (curve 4 in Fig. 2). The line intensities are much lower. The intercombination line is not observed on the background, which complicates the quantitative analysis of this data. Let's notice that the reduction of X-ray generation with the SiO_2-aerogel target can also be due in part to the increased transparency and reduced coupling with the incident laser frequency (working at the 4th harmonics of Nd laser should increase the coupling dramatically).

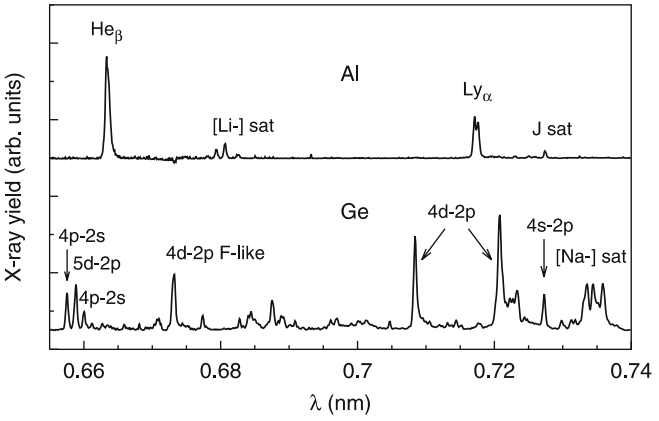

FIGURE 3 Experimentally observed X-ray spectra of the Al (*upper curve*) and Ge (*lower curve*) laser-produced plasmas (the second harmonic). See Table 1 for the line notation

Figure 3 shows the experimentally observed spectra for the Al and Ge plasmas obtained with the second harmonic. Measurements were performed with a single RAR film in the spectral region of the Ly_α and He_β lines of Al and their dielectronic satellites. The line labeling and spectroscopic constants of corresponding transitions are given in Table 1.

The results shown in Figs. 2 and 3 were analysed to obtain the plasma parameters. Note that the observations are time integrated, thus only average values can be estimated. We used the calculated intensities of the Ly_α and $He_{\alpha 1}$ lines and their dielectronic satellites [20] to obtain the electron temperatures of the Al and Si plasmas. These calculations confirm previous theoretical results [21] and agree well with calculations from a corona model [22].

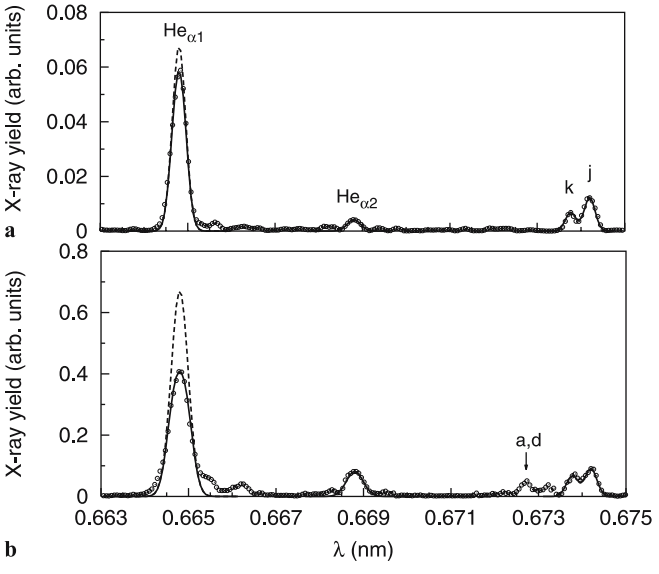

FIGURE 4 Comparison of calculations according to (1) with experimentally observed spectrum (open circles) in the region of the $He_{\alpha 1}$ and *j*-satellite lines for the glass target (**a**) and the pure silicon target (**b**). *Solid curves* for the $He_{\alpha 1}$ line are calculations with account of plasma opacity. *Dashed curves* correspond to optically thin plasma

3.2 *Analysis of the* $\mathbf{He_\alpha}$ *and dielectronic satellite lines in* Si *plasma*

Figure 4 shows the spectral region of the $He_{\alpha 1}$ and (k, j) satellite lines for glass and pure Si targets. For the glass target (Fig. 4a), the k and j satellites are spectrally resolved. For the pure Si, they are partly blended. However, their widths and intensities can still be determined. The plasma is optically thin for these lines. The difference of their widths observed with these targets can be explained by the different values of the ion temperature, because the total line width is mainly determined by Doppler broadening and the instrumental width. The total line widths for the satellite lines and the corresponding ion temperatures, estimated after subtraction of the instrumental width, are given in Table 2.

Our plasma is also optically thin for the intercombination line $He_{\alpha 2}$. However, this line is broader than the satellites. The reason may be due to different emission times. The satellites are radiated during the beginning period of the plasma expansion, while for the $He_{\alpha 2}$ line the later stages dominate in the radiation yield corresponding to the higher effective ion temperature and Doppler width.

The observed resonance line $He_{\alpha 1}$ is broader than the intercombination line. However for the modeling, we use the same width as for the $He_{\alpha 2}$ line. The difference is due to plasma opacity for the resonance line. The absorption effect in the line shape of the $n \to 1$ transitions can be accounted for by using the uniform plasma layer approximation

$$I_{n1}(\lambda) = \frac{I_{n1}}{\tau_{n1}} \left[1 - \exp\left(-\tau_{n1} S_{n1}(\lambda)\right)\right] \tag{1}$$

where

$$\tau_{n1} = \frac{\lambda_{n1}^4}{4} \frac{A_{n1} g_n / g_1}{\pi^{3/2} c \Delta\lambda_D} N_1 L \tag{2}$$

is the optical depth at the line centre, g_n is the statistical weight of the level n, $\Delta\lambda_D$ is the Doppler line width, N_1 is the ground state population coefficient, L is the layer size, and $S_{n1}(\lambda) = \exp[-(\lambda - \lambda_{n1})^2/(\Delta\lambda_{n1}/2)^2]$ is the line-profile function for an optically thin plasma with the total line width $\Delta\lambda_{n1} = (\Delta\lambda_D^2 + \Delta\lambda_{instr}^2)^{1/2}$.

The results of line profile calculations for the optically thin and optically thick plasmas are shown in Fig. 4. The values of I_{n1} and τ_{n1} for the $He_{\alpha 1}$ line were obtained by fitting formula (1) to the observed spectral intensity. The width was obtained from the $He_{\alpha 2}$ line profile. The fitting gives a low value of the plasma opacity for the $He_{\alpha 1}$ line for the glass target (see Fig. 4a). The measured width is close to that of the intercombination line. In contrast, the $He_{\alpha 1}$ line in pure Si plasma is more strongly reabsorbed, as can be seen from Fig. 4b. One of the reasons is the lower number density of Si ions in the plasma from glass targets (N_{Si}) as compared to the density of Si ions in the plasma from pure silicon targets (N'_{Si}) in correspondence of the same value of the electron density

$$N'_{Si} = \frac{Z_{Si} + Z_O N_O / N_{Si}}{Z'_{Si}} N_{Si} , \tag{3}$$

where Z_{Si} and Z'_{Si} are the average charge of the silicon ions in the glass and pure Si plasmas, respectively, $N_O \approx 2N_{Si}$ and $Z_O = 8$ are the density and the ion charge for completely ionized oxygen at the electron temperature typical for the He-like silicon ions. Thus, $N'_{Si} \approx 2.3 N_{Si}$ as follows from (3) at $Z'_{Si} \approx Z_{Si} \approx 12$. However, this difference can explain only the decrease of the total line intensity (by a factor of about two), but not the plasma opacity. An actual ion charge distribution should be taken into account.

The peak values of line intensities for optically thin plasmas obtained from the modeling were used to estimate the total intensity ratio for the j satellite and $He_{\alpha 1}$ lines in the form

$$R(j, \alpha 1) = \frac{I_j \Delta\lambda_j}{I_{\alpha 1} \Delta\lambda_\alpha} \tag{4}$$

and the results were compared with calculations [20].

According to [20], the main channel through which corresponding autoionizing states in the Li-like silicon ion are populated, is the dielectronic capture. Thus the intensity ratio (4) depends only on the electron temperature, but not on the electron density. The electron temperature values corresponding to the intensity ratio for different targets and laser harmonics used in the experiments are shown in Table 2.

The electron densities shown in Table 2 were obtained from the resonance and intercombination line intensity ratio $R(\alpha 1, \alpha 2) = I_{\alpha 1}/I_{\alpha 2}$, corrected for the plasma opacity, by comparison with the level kinetic calculations for optically thin plasma presented in [12]. The optical depth gives from (2) the value of the effective plasma layer thickness, i.e., the product of the ground state population coefficient N_1, and the layer size L. Note that the Ly_α line of the H-like silicon ion was not observed in these spectral measurements. It follows from the value of the He-like silicon ionization rate by the electron bulk. According to the Lotz formula, the ionization time is $\tau_{ion} \approx 8$ ns at $T_e = 500$ eV and $N_e = 10^{21}$ cm^{-3}; that is much larger than the pulse duration and larger than the average plasma decay time, $\Delta t_{dec} \approx 1$ ns, estimated from the observed size of the emission zone and the average ion velocity of $\sim 10^7$ cm/s. The ionization time for the Li-like ion, $\tau_{ion} \approx 20$ ps, is of the order of the laser pulse duration.

Parameter		Target (laser harmonic)		
		SiO_2 (1ω)	Si (1ω)	Si (2ω)
j-satellite	$\Delta\lambda$ (pm)	0.35	0.4	0.5
	T_i (keV)	0.52	0.78	1.43
$He_{\alpha 1}$	$\Delta\lambda$ (pm)	0.43	0.55	0.62
	T_i (keV)	1.0	1.9	2.5
$\tau_{\alpha 1}$		0.3	1.1	3.9
$N_{He} L$ (10^{16} cm^{-2})		0.34	1.7	6.8
$I_j \Delta\lambda_j / (I_{\alpha 1} \Delta\lambda_{\alpha 1})$		0.145	0.10	0.093
T_e (eV)		460	550	560
$I_{\alpha 1}/I_{\alpha 2}$		16.3	8.3	10.8
N_e (10^{21} cm^{-3})		1.9	1.05	1.4

TABLE 2 The line widths and line intensity ratios in Si plasmas of different targets and corresponding plasma parameters

3.3 *Ly*$_\alpha$ *line and its satellites* Al *plasma*

In Al plasmas, the Ly_α line of the H-like ion and J dielectronic satellites are observed. The results of the line modeling are shown in Fig. 5 and compared to the measured spectrum. The fine structure of the Ly_α line is clearly resolved,

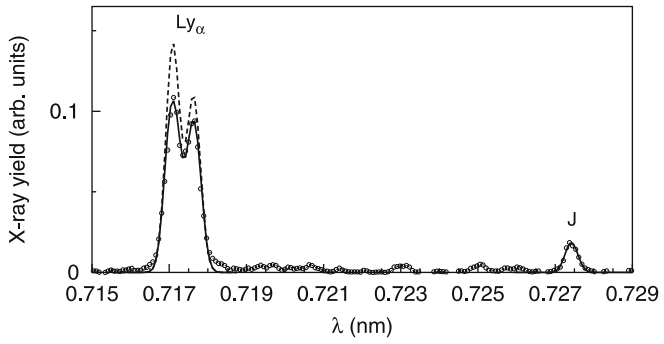

FIGURE 5 Comparison of the experimentally observed spectrum (*open circles*) and calculations according to (5) for the Al target in the region of the Ly$_\alpha$ and J-satellite lines. The *dashed curve* is for the optically thin plasma, the *thick full curve* is for the optical depth $\tau_{1/2} = 0.3$ and the population ratio $N_{3/2}/N_{1/2} = 1.3$

and the intensities of two components with the total angular momentum $j = 3/2$ and $1/2$ can be obtained. For level populations in statistical equilibrium, the component intensity ratio is 2, while the experimental value is 1.3. Because in our spectra the Lamb shift is not resolved, this difference can be explained by the Stark mixing of the $2s_{1/2}$ and $2p_{3/2}$ states that redistributes the transition probability in favor of the forbidden transition. Another possibility is the depopulation of the metastabel $2s_{1/2}$ state to the $2p_{1/2}$ level by electronic collisions. Both effects result in an increase of the $2p_{1/2} \to 1s_{1/2}$ intensity with respect to the $2p_{3/2} \to 1s_{1/2}$ intensity.

The intensities for the overlapped optically thick lines were calculated using the following modification of (1)

$$I_{21}(\lambda) = I_{21}\frac{rS_{3/2}(\lambda) + S_{1/2}(\lambda)}{\tau_{3/2}S_{3/2}(\lambda) + \tau_{1/2}S_{1/2}(\lambda)} \times \left[1 - \exp\left(-\tau_{3/2}S_{3/2}(\lambda) - \tau_{1/2}S_{1/2}(\lambda)\right)\right] , \qquad (5)$$

where $\tau_{1/2}$ and $\tau_{3/2} = 2\tau_{1/2}$ are the optical depths of the Ly$_\alpha$ line components $j = 1/2$ and $3/2$, respectively, and $r = N_{3/2}/N_{1/2}$ is the ratio of population coefficients.

The J satellite is narrower than the resonance Ly$_\alpha$ line (as in the Si plasma). Following calculations in [10], the observed intensity ratio for these lines of about 0.067 gives an electron temperature of $T_e \approx 560$ eV, that is slightly higher than that for Si plasmas (see Table 2).

A similar analysis of the He$_\beta$ line gives an optical depth $\tau_{He\beta} \approx 1.2$, larger than that of the Ly$_\alpha$ line ($\tau_{1/2} \approx 0.3$). As the transition probability of the He$_\beta$ line is smaller and its line width larger, the population of the H-like ion should then be much lower than that of the He-like ion. The ionization time for the He-like ion at $T_e = 560$ eV and $N_e = 10^{21}$ cm^{-3} ($\tau_{ion} \approx 0.6$ ns) is smaller than the plasma decay time. In this case, the excited levels are populated mainly due to the electron excitation from the ground state. Unfortunately, the He$_\alpha$ lines were not measured here and the electron density for the Al plasma could not be determined in the same manner as for the Si plasma. However, its value is expected to be nearly the same.

3.4 *X-ray radiation from the laser–plasma source*

We assume that the X-ray emission from the plasma is isotropic. Alternatively, the angular distribution can be described by the cos β dependence where β is the angle between the ray considered and the direction normal to the target surface (see, e.g., [23]). However, a possible X-ray anisotropy is negligible here because the corresponding correction factor for the yield is less than 2.

The number of photons that exposing the film is the integral over the plasma decay period Δt_{dec}, the line width $\Delta\lambda$ and the emission solid angle corresponding to the crystal aperture (after subtracting of the background). For isotropic emission it reads

$$\Delta N_{det} = N_{em}\tau_f\varrho_c\frac{\Delta\Omega}{4\pi} , \qquad (6)$$

where $\tau_f(\lambda)$ is the filter transmission, $\varrho_c(\lambda)$ is the quartz crystal reflectivity, $N_{em} = n(\lambda, t)\Delta\lambda\Delta t_{dec}$ is the total number of photons emitted within the line width during the decay period, $n(\lambda, t) \equiv d^2N/(\mathrm{d}\lambda\,\mathrm{d}t)$ is the spectral emission rate. The crystal aperture angle in the spectral and spatial directions is

$$\Delta\Omega = \frac{\Delta x\Delta y}{a^2} , \qquad (7)$$

where a is the distance from the plasma region to the crystal centre, $\Delta y = y_c$ is the crystal size in the direction transverse to the dispersion plane (the focusing effect). Δx can by obtained geometrically from

$$\Delta x = \frac{Ra\cos\theta}{a - R\sin\theta}\frac{\Delta\lambda}{\lambda} . \qquad (8)$$

Here R is the crystal radius, $\theta = \arcsin(\lambda/2d)$ is the Bragg reflection angle (in the first order) corresponding to the wavelength λ and d is the distance between symmetric layers in the crystal.

Using (8), the crystal aperture (7) reads

$$\Delta\Omega = \frac{R\cos\theta}{a - R\sin\theta}\frac{y_c}{a}\frac{\Delta\lambda}{\lambda} . \qquad (9)$$

From (6) and (9) one can estimate the total number of photons in the line emitted in the solid angle 2π

$$N_{em} = \frac{2\pi a\lambda(a - R\sin\theta)}{\tau_f\varrho_c y_c\Delta\lambda R\cos\theta}\Delta N_{det} . \qquad (10)$$

Table 3 shows the results for different spectral lines in Al, Si, and Ge plasmas corresponding to the experimental arrangement ($a = 230$ mm, $y_c = 8$ mm and $d = 0.425$ nm). Absolute values of the exposure were obtained using the X-ray response data for the RAR film from [24].

Line and Ion	λ (nm)	$\Delta\lambda$ (nm)	N_{em} (10^{12})	$\Delta\Omega$ (10^{-5}sr)
He$_{\alpha 1}$ Si^{+12}	0.6648	0.0006	2.5	1.1
Ly$_\alpha$ Al^{+12}	0.7172	0.001	0.6	1.8
He$_\beta$ Al^{+11}	0.663	0.0005	1.3	1.1
$2p^5 4s - 2p^6$Ge^{+22}	0.708	0.0007	1.2	1.2

TABLE 3 Total number of photons in different spectral lines emitted in the solid angle 2π by 40-ps laser-produced plasmas and corresponding crystal aperture angle (9)

From these estimations, it follows that about 10^9 X-ray photons per laser pulse are available on a sample surface of $1\,\mathrm{cm}^2$ at the distance 10 cm from the plasma source in the bandwidth $\Delta\lambda/\lambda \approx 0.05$. The total X-ray yield from several lines increases the photon number irradiating a sample by an order of magnitude. In this case, L-shell emitters like Ne-like Cu would be preferable due to their higher X-ray yield [17]. Another way to increase the X-ray flux on a sample is to use the focusing property of a spherical crystal spectrometer [25]. With the additional focusing, the X-rays flux is about 10^{13} photons/cm^2 in a 1-mm diameter spot per a laser pulse.

4 Conclusions

We have performed high-precision X-ray spectroscopy studies of plasmas produced by 40-ps pulses from a small Nd:YAG laser system. The beam was focused on different targets (Al, SiO_2-aerogel, SiO_2, and Si). Spectral line profiles and intensities of the resonance transitions in the H-like and He-like aluminum and silicon ions and their dielectronic satellite lines have been analyzed to obtain the electron density, N_e, and electron temperature, T_e, of the pertaining plasmas. The analysis yields $T_e = (460-560)$eV and $N_e = (1.0-1.9)\times 10^{21}\,\mathrm{cm}^{-3}$ in Si plasmas and $T_e \approx 560$ eV in Al plasmas for the first and second laser harmonics. In the case of Al plasmas, the He_α lines were not measured but the electron density is expected to be nearly the same ($N_e \approx 10^{21}\,\mathrm{cm}^{-3}$). The plasma opacity was taken into account to correctly compare the experimentally observed resonance line intensities with those obtained theoretically for an optically thin plasma.

The laser-produced plasma studied seems to be a promising source of soft X-ray radiation. The total number of photons emitted in the resonance lines from a plasma region of about 100-μm size during the decay period is about 10^{13}, which it makes possible to use it as a point-like bright X-ray source.

ACKNOWLEDGEMENTS We thank Moreno Piselli, Università di Milano-Bicocca, for the technical help in the experiment and for realizing the interaction chamber used in the experiment. A.I. Magunov gratefully acknowledges the hospitality of the University of Milano-Bicocca and the support by the FEMTO Programme of the European Scientific Foundation. This work was partly supported by INTAS project 01–0233.

REFERENCES

1 E. Turcu, G.J. Tallents, I. Ross, A.G. Michette, M. Schulz, R.A. Meldrum, C.W. Wharton, D. Batani, M. Martinetti, A. Mauri, Phys. Medica **10**, 93 (1994)
2 A. Masini, D. Batani, F. Previdi, M. Costato, A. Pozzi, E. Turcu, R. Allott, N. Lisi, Eur. Phys. J. – Appl. Phys. **5**, 101 (1999)
3 M. Milani, A. Conte, M. Costato, F. Salsi, G. Baroni, D. Batani, L. Ferrario, E. Turcu, Eur. Phys. J. D **5**, 267 (1999)
4 F. Bortolotto, D. Batani, F. Previdi, L. Rebonato, E. Turcu, Eur. Phys. J. D **11**, 309 (2000)
5 D. Batani, C. Botto, F. Bortolotto, A. Masini, A. Bernardinello, M. Moret, G. Poletti, F. Cotelli, C. Lora Lamia Donin, S. Piccoli, A. Stead, T. Ford, A. Marranca, K. Eidmann, F. Flora, L. Palladino, L. Reale, Phys. Medica **14**, 49 (2000)
6 D. Batani, C. Botto, A. Bernardinello, M. Moret, F. Cotelli, C. Lora Lamia Donin, A. Stead, T. Ford, K. Eidmann, Eur. Phys. J. D **21**, 167 (2002)
7 T. Desai, D. Batani, A. Bernardinello, G. Poletti, F. Orsini, J. Ullschmied, L. Juha, J. Skala, B. Kralikova, E. Krousky, M. Pfeifer, C. Kadlec, T. Mocek, A. Präg, O. Renner, F. Cotelli, C. Lora Lamia Donin, A. Zullini, Laser Part. Beams **21**, 509 (2003)
8 G. Poletti, F. Orsini, D. Batani, A. Bernardinello, T. Desai, J. Ullschmied, J. Skala, B. Kralikova, E. Krousky, M. Pfeifer, C. Kadlec, T. Mocek, A. Präg, O. Renner, F. Cotelli, C. Lora Lamia Donin, A. Zullini, Eur. Phys. J. D **24**, 84 (2004)
9 E. Turcu, J.R. Maldonado, I. Ross, H. Shields, P. Trenda, D. Batani, P. Fluck, H. Goodson, Microelectron. Eng. **23**, 243 (1994)
10 F. Bijkerk, E. Louis, M. Van derWiel, E. Turcu, G.J. Tallents, D. Batani, J. X-ray Sci. Technol. **3**, 133 (1992)
11 V.A. Boiko, S.A. Pikuz, U.I. Safronova, A.Y. Faenov, Mon. Not. R. Astron. Soc. **185**, 789 (1978)
12 V.A. Boiko, S.A. Pikuz, A.Y. Faenov, J. Phys. B **12**, 1889 (1979)
13 I.Yu. Skobelev, A. Bartnik, E. Behar, R. Doron, V.M. Dyakin, J. Kostecki, P. Mandelbaum, A.Ya. Faenov, H. Fiedorowicz, J.L. Schwob, M. Szczurek, R. Jarocki, Quantum Electron. **28**, 677 (1998)
14 F.B. Rosmej, A.Ya. Faenov, T.A. Pikuz, F. Flora, P.Di Lazzaro, T. Letardi, A. Grilli, A. Reale, J. Phys. B – At. Mol. Opt. **31**, L921 (1998)
15 F.B. Rosmej, D.H.H. Hoffmann, W. Süß, M. Geißel, A.Ya. Faenov, T.A. Pikuz, Phys. Rev. A **63**, 032 716 (2001)
16 V.S. Belyaev, V.I. Vinogradov, A.S. Kyrilov, A.I. Magunov, A.P. Matafonov, T.A. Pikuz, I.Yu. Skobelev, A.Ya. Faenov, JETP **96**, 897 (2003)
17 A. Faenov, T. Pikuz, A. Magunov, D. Batani, G. Lucchini, F. Canova, M. Piselli, Laser Part. Beams **22**, 373 (2004)
18 I.Y. Skobelev, A.Y. Faenov, B.A. Bryunetkin, V.M. Dyakin, T.A. Pikuz, S.A. Pikuz, T.A. Shelkovenko, V.M. Romanova, A.R. Mingaleev, JETP **81**, 692 (1995)
19 G. Holzer, O. Wehrhan, E. Forster, Cryst. Res. Technol. **33**, 555 (1998)
20 U.I. Safronova, A.M. Urnov, L.A. Vainshtein, Preprint of Lebedev Physical Institute, No. 212 (1978)
21 C.P. Bhalla, A.H. Gabriel, L.P. Presnyakov, Mon. Not. R. Astron. Soc. **172**, 359 (1975)
22 V.L. Jacobs, M. Blaha, Phys. Rev. A **21**, 525 (1980)
23 E. Turcu, M.C. Gower, C.J. Reason, P. Huntington, M. Schulz, A.G. Michette, F. Bijkerk, E. Louis, G. Tallents, Y. Al-Hadithi, D. Batani, "100 Hz KrF Laser-Plasma X-ray Source" In: *Excimer Lasers and Applications III* SPIE Vol. 1503, pp. 391–405, USA (1991)
24 B.L. Henke, F.G. Fujiwara, M.A. Tester, C.H. Dittmore, M.A. Palmer, J. Opt. Soc. Am. B **1**, 828 (1984)
25 T.A. Pikuz, A.Y. Faenov, M. Fraenkel, A. Zigler, F. Flora, S. Bollanti, P. Di Lazzaro, T. Letardi, A. Grilli, L. Palladino, G. Tomassetti, L. Reale, T. Limongi, F. Bonfigli, Proc. SPIE-99, Vol. 3767. Denver-99, pp. 67–79
26 G. Vergunova, A. Magunov, V. Dyakin, A. Faenov, T. Pikuz, I. Skobelev, D. Batani, S. Bossi, A. Bernardinello, F. Flora, P. Di Lazzaro, S. Bollanti, N. Lisi, T. Letardi, A. Reale, L. Palladino, A. Scafati, L. Reale, A. Osterheld, W. Goldstein, Phys. Scripta **55**, 483 (1997)
27 F. Rosmej, A. Faenov, T. Pikuz, F. Flora, P. Di Lazzaro, S. Bollanti, N. Lisi, T. Letardi, A. Reale, L. Palladino, D. Batani, S. Bossi, A. Bernardinello, A. Scafati, L. Reale, A. Zigler, M. Fraenkel, E. Cowan, J. Quant. Spectrosc. Radiat. Transfer **58**, 859 (1997)
28 E. Biemont, A.I. Magunov, V. Dyakin, A. Faenov, T. Pikuz, I. Skobelev, A. Osterheld, W. Goldstein, F. Flora, P. Di Lazzaro, S. Bollanti, N. Lisi, T. Letardi, A. Reale, L. Palladino, D. Batani, A. Mauri, A. Scafati, L. Reale, J. Phys. B – At. Mol. Opt. **33**, 2153 (2000)
29 A. Magunov, A. Faenov, I. Skobelev, T. Pikuz, D. Batani, M. Milani, M. Costato, A. Pozzi, E. Turcu, R. Allot, M. Koenig, A. Benuzzi, F. Flora, A.Reale, Laser Part. Beams **16**, 61 (1998)
30 D. Batani, M. Koenig, A. Benuzzi, J.M. Boudenne, G. Cauchon, T. Hall, W. Nazarov, Rev. Sci. Instrum. **70**, 1464 (1999)
31 F. Pisani, M. Koenig, D. Batani, T. Hall, D. Desenne, J. Bruneau, C. Reverdin, Rev. Sci. Instrum. **70**, 3314 (1999)
32 M. Koenig, J.M. Boudenne, P. Legriel, T. Grandpierre, D. Batani, S. Bossi, S. Nicolella, R. Benattar, Rev. Sci. Instrum. **68**, 2387 (1997)